

AutoDriDM: An Explainable Benchmark for Decision-Making of Vision-Language Models in Autonomous Driving

Zecong Tang^{1,*} Zixu Wang^{1,*} Yifei Wang^{1,*} Weitong Lian^{1,*}
 Tianjian Gao¹ Haoran Li¹ Tengju Ru¹ Lingyi Meng¹
 Zhejun Cui¹ Yichen Zhu¹ Qi Kang¹ Kaixuan Wang² Yu Zhang^{1,†}

¹Zhejiang University, Hangzhou, China

²The University of Hong Kong, Hong Kong, China

*Equal contribution †Corresponding author

Abstract

Autonomous driving is a highly challenging domain that requires reliable perception and safe decision-making in complex scenarios. Recent vision-language models (VLMs) demonstrate reasoning and generalization abilities, opening new possibilities for autonomous driving; however, existing benchmarks and metrics overemphasize perceptual competence and fail to adequately assess decision-making processes. In this work, we present **AutoDriDM**, a decision-centric, progressive benchmark with 6,650 questions across three dimensions—Object, Scene, and Decision. We evaluate mainstream VLMs to delineate the perception-to-decision capability boundary in autonomous driving, and our correlation analysis reveals weak alignment between perception and decision-making performance. We further conduct explainability analyses of models’ reasoning processes, identifying key failure modes such as logical reasoning errors, and introduce an analyzer model to automate large-scale annotation. AutoDriDM bridges the gap between perception-centered and decision-centered evaluation, providing guidance toward safer and more reliable VLMs for real-world autonomous driving.

1 Introduction

Autonomous driving is a highly challenging domain operating under diverse and safety-critical conditions. Research has progressed along two main paradigms. The first, a modular pipeline, separates perception, prediction/planning, and control (Schwarting et al., 2018; Badue et al., 2021; Paden et al., 2016). The second, end-to-end learning, maps raw sensor inputs directly to waypoints or control commands (Tampuu et al., 2022; Chen et al., 2024a; Codevilla et al., 2018). While both approaches have achieved notable success, modular systems remain brittle due to error propagation, whereas end-to-end methods often lack explainability and robust reasoning about causal structure

(Badue et al., 2021; Chib and Singh, 2023).

The development of large language models (LLMs) has enabled significant advances in instruction following and reasoning (OpenAI et al., 2024; Touvron et al., 2023; DeepSeek-AI et al., 2025). In parallel, vision-language models (VLMs) have emerged with capabilities in zero-shot transfer and language-based reasoning (Zhang et al., 2024; Shen et al., 2024; Lu et al., 2025). These properties highlight the potential of VLMs for autonomous driving; domain-specific VLM-based systems for autonomous driving have been proposed (Zhou et al., 2024a; Tian et al., 2024; Fu et al., 2024b; You et al., 2025), demonstrating increasing research activity and diverse approaches.

Despite these advancements, current approaches face several limitations. Benchmarks serve as a bridge between methodological advances and practical deployment by revealing model failures. First, existing VLM training primarily focuses on perception, overlooking the decision-making requirements of driving scenarios (Zhou et al., 2024b), which is a core component for fully autonomous driving. Second, many benchmarks define independent metrics that decouple perception from the decisions they should support, limiting the assessment of models’ true capability boundaries (Xie et al., 2025). Third, evaluations often consider only final answers, making reasoning error a black box, which constrains analysis of performance gaps (Li et al., 2025; Guo et al., 2024).

To address these limitations, we introduce AutoDriDM (Figure 1), a decision-centric benchmark for evaluating VLMs in autonomous driving. First, AutoDriDM is constructed from nuScenes, KITTI, and BDD100K and follows a three-level protocol with increasing task complexity — Object, Scene, and Decision. The benchmark comprises 6.65K questions across six metrics, with evaluations stratified by scenario risk. To further assess robustness, we curate 60 pairs of visually similar scenar-

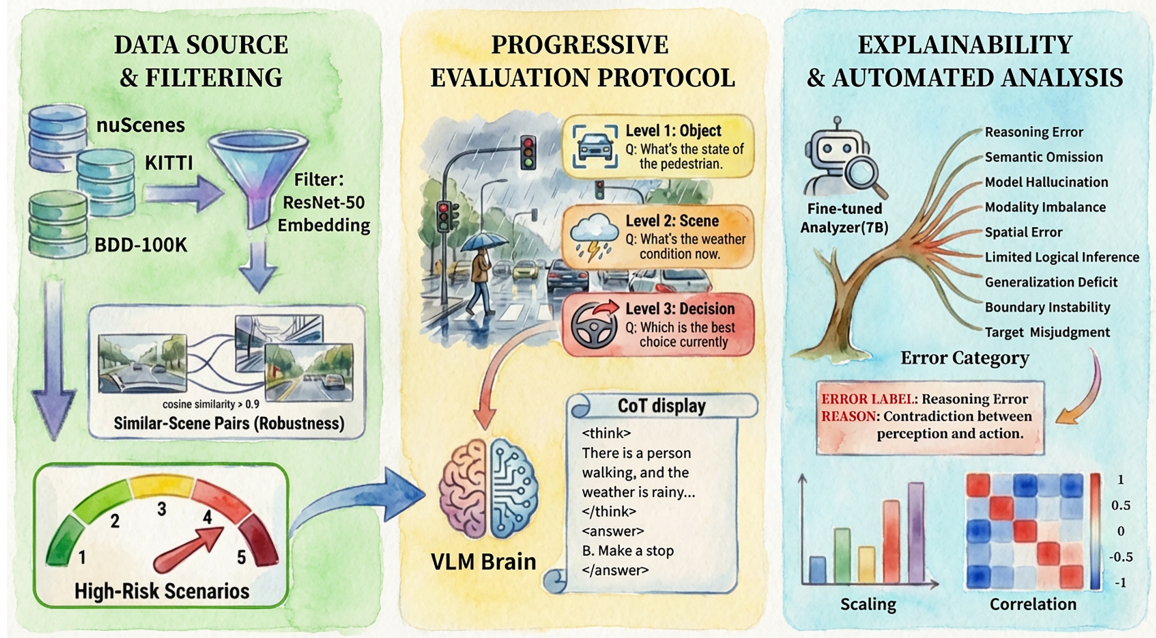


Figure 1: Overview of AutoDriDM. The framework is organized into three stages: (Left) Data Source & Filtering, (Middle) Progressive Evaluation Protocol, and (Right) Explainability & Automated Analysis.

ios. Second, we evaluate mainstream open- and closed-source VLMs to characterize their capability boundaries under zero- and few-shot settings, and quantify cross-level dependencies between perception and decision-making through correlation analysis. Moreover, we investigate the scaling behavior of the Internvl models, identifying key inflection points. Third, we collect and annotate reasoning traces from multiple VLMs to conduct systematic analyses of their reasoning and failure patterns. Based on this analysis, we fine-tune a lightweight analyzer model to automatically tag new traces, enabling scalable evaluation and providing insights for model optimization.

Our work makes three key contributions:

- We introduce AutoDriDM, a decision-centric benchmark with a progressive three-level protocol—Object, Scene, and Decision—covering 6.65K questions with six evaluation metrics and risk-aware splits.
- We evaluate mainstream VLMs, analyze perception–decision dependencies, study robustness on visually similar scenarios, and investigate the scaling behavior of Internvl models to identify key inflection points.
- We collect and annotate reasoning traces from VLMs, analyze these traces to reveal reasoning and failure patterns, and fine-tune a model to automate reasoning trace labeling, enabling large-scale explainability.

2 Related Work

2.1 VLMs for Autonomous Driving

Recent advances in LLMs have accelerated the development of VLMs (OpenAI et al., 2024; Touvron et al., 2023; DeepSeek-AI et al., 2025; Zhao et al., 2023). VLMs leverage large-scale image–text pre-training and instruction tuning, demonstrating robust instruction-following, zero-shot generalization, and contextual reasoning capabilities (Li et al., 2023; Wang et al., 2024a; Lu et al., 2025). They have been extensively investigated in autonomous driving for scene understanding, interactive reasoning, and end-to-end planning (Zhou et al., 2024a; Tian et al., 2024; Xu et al., 2024; Sima et al., 2025; You et al., 2025; Fu et al., 2024b; Gopalkrishnan et al., 2024). However, current VLMs still suffer from hallucinations, brittle reasoning, and omissions of critical visual cues in complex scenes (Guan et al., 2024; Yu et al., 2024; Bai et al., 2025).

2.2 Benchmarks for LLMs/VLMs

For LLMs, mainstream benchmark suites evaluate knowledge, reasoning, and math/coding abilities using more challenging protocols and adversarial design (Wang et al., 2024b; Rein et al., 2024; Sakaguchi et al., 2021; Clark et al., 2018; Chen et al., 2021; Patel et al., 2024). For VLMs, general-purpose evaluations aim to assess comprehensive capabilities across perception, grounding,

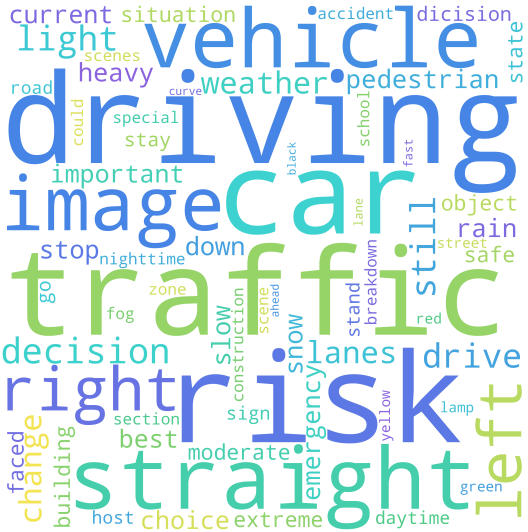


Figure 2: The word cloud about autonomous driving collected from our QA pairs in AutoDriDM.

OCR/text reasoning, and hallucination robustness (Fu et al., 2024a; Liu et al., 2024a; Yu et al., 2024; Yue et al., 2024, 2025; Guan et al., 2024; Liu et al., 2024b; Tang et al., 2025; Mathew et al., 2021; Zhang et al., 2025). In autonomous driving, recent VLM-oriented benchmarks provide driving scenes and tasks for perception–planning evaluation (Guo et al., 2024; Li et al., 2024, 2025; Sima et al., 2025); however, most employ independent metrics, with insufficient analysis of model reasoning traces.

3 AutoDriDM

This section introduces our comprehensive decision-making–centered benchmark framework for evaluating VLMs in autonomous driving.

3.1 Data Source and Filtering

Data source. We construct our benchmark from three widely used driving datasets—nuScenes, KITTI, and BDD100K (Caesar et al., 2020; Geiger et al., 2013; Yu et al., 2020)—focusing on front-facing images. The integration of these datasets spans multiple regions and diverse driving environments. This diversity mitigates dataset-specific bias and enhances the coverage of real-world driving conditions. Since we attach multiple task-specific questions to the same driving scene, a single image may correspond to multiple questions across different tasks; Appendix A.1 summarizes the dataset profiles (regions, scene types, and task coverage) together with the image / QA usage statistics.

Data filtering. For quality control, we employ a similarity-based filtering procedure. We compute

image embeddings using a pretrained ResNet-50 (He et al., 2016) with global average pooled representations and construct candidate pairs based on cosine similarity. Pairs exceeding a similarity threshold of 0.9 are treated as near-duplicate cases and removed to reduce redundancy.

3.2 Benchmark Construction

We adopt a three-level protocol, comprising Object, Scene, and Decision, which is progressively structured rather than independent: perception supports scene understanding, and both stages jointly inform decision-making.

Overview. We define two metrics at each level, thereby establishing an Object–Scene–Decision evaluation pipeline. All metrics are selection questions: Object and Decision are single-choice, while Scene is multiple-choice. The benchmark contains **6.65K** questions covering the three levels. Figure 2 shows a word cloud for our benchmark. Detailed annotation templates for all six tasks are provided in Appendix C.5.

Object level evaluates perception: (Object-1) identify the object in the image that most influences the decision; (Object-2) determine the state of a designated object. **Scene level** aims to evaluate scene-level understanding: (Scene-1) recognize weather and illumination; (Scene-2) identify special scene factors that potentially influence driving decisions (e.g., roadworks, accidents). **Decision level** aims to evaluate decision-making capability: (Decision-1) select the optimal action for the ego vehicle in the scenario; (Decision-2) evaluate the safety of specified and potentially suboptimal actions. Both tasks are informed by critical perceptual and contextual signals from Object-1/2 and Scene-1/2, providing the basis and constraints for decision-making. We summarize the design intentions of the six tasks in Appendix A.2.

Annotation protocol. To ensure annotation accuracy, all QA pairs are manually annotated by human annotators. To ensure annotation consistency, each item is independently labeled by two experienced drivers. In cases of disagreement, a third human arbitrator adjudicates, and the final annotation is assigned accordingly.

High-risk scenario design. Due to the scarcity of high-risk scenarios, collecting sufficient data for these cases can be challenging and may limit the pretraining of VLMs. However, these scenarios are critical for safe driving, and thus we evaluate them to assess the generalization capability of VLMs.

Each scenario is rated by two expert annotators using a five-point risk scale (1: minimal, 5: severe, see Appendix A.3). The average score is used as the final rating, and scenarios with a score of 4 or higher are designated as high-risk scenarios, resulting in a total of **1.6K** questions for analysis.

Similar-scene robustness. Humans can identify task-relevant information and ignore redundant cues, enabling accurate decision-making in visually similar scenarios. To test whether models exhibit this fine-grained capability, we construct **60** near-duplicate pairs based on similarity filtering in Sec. 3.1. We evaluate model performance on Decision-1 using both the single-image accuracy and the joint accuracy (the probability that both images in a pair are answered correctly). Comparison with the squared baseline of individual accuracies evaluates whether decisions reflect causal understanding rather than superficial feature associations, thereby assessing VLMs’ robustness in causal reasoning. Representative near-duplicate examples are provided in Appendix A.4.

Correlation analysis. Benefiting from our three-level design (Object, Scene, and Decision), which establishes a progressive rather than independent structure, we explore the internal consistency of model behavior across perception and decision dimensions by computing pairwise Pearson correlations among all task scores for each model. This analysis reveals whether enhancements in one capability co-occur with gains or trade-offs in others. The resulting correlation matrices provide evidence for the multimodal reasoning across cognitive stages within VLMs.

3.3 Explainability Settings

We analyze the reasoning process of VLMs by classifying errors and fine-tune a lightweight model to scale up analysis for automated evaluation.

Model reasoning. Chain-of-thought (CoT) reasoning has been shown to improve problem-solving capability (Wei et al., 2022) and reveal intermediate dependencies that determine the final choice. To leverage these advantages, we instruct the model to generate a structured CoT rationale enclosed within `<think>...</think>`, followed by the decision enclosed within `<answer>...</answer>` in a single-turn interaction. This configuration facilitates fine-grained analysis across the Object, Scene, and Decision levels, and allows a more precise assessment of the model’s upper-bound capability.

Error categories. We define nine error cat-

egories (E1–E9) to characterize failures across the decision-making process, following the taxonomy in Appendix B.1. The three primary categories are (E1) Logical Reasoning Error (the reasoning chain violates causality), (E2) Semantic Feature Omission (the model overlooks or misjudges semantic/visual cues such as turn signals), and (E3) Model Hallucination (the model invents non-existent objects, attributes, or relations). The remaining categories are (E4) Modality Imbalance, (E5) Spatial Relation Misjudgment, (E6) Limited Logical Inference, (E7) Generalization Deficit, (E8) Decision Boundary Instability, and (E9) Target Priority Misjudgment.

Automated reasoning-mode tagging. Analyzing the explainability process manually is resource-intensive and constrains scalability. To enable automated large-scale evaluation, we train a lightweight analyzer model with 7B parameters that identifies error modes. The model takes as input: (1) the image, question, options, and ground-truth answer; (2) the tested model’s reasoning and final answer. It outputs one or more error-mode labels from the nine defined error categories, or a no-error label otherwise. This approach enables scalable error-type identification, and supports systematic evaluation of model reasoning. The analyzer input/output format and the prompt templates are provided in Appendix B.2.

4 Experiments

4.1 All Scenarios Results (0-shot)

We analyzed the overall results to evaluate the general capability strengths. GPT-4.1 ranks first in overall performance, while among open-source models, Qwen (72B) yields the highest average performance. Although closed-source models continue to demonstrate superior generalization and stability, recent open-source systems show growing competitiveness. Representative failure cases of GPT-4.1 are shown in Figure 3. Complete 0-shot results are presented in Table 1. Experimental setup is shown in Appendix C.1.

The results exhibit a clear stratification: larger-scale models generally achieve higher accuracy on Object-1/2 and perform more consistently on Scene-1, while models under 10B parameters exhibit higher performance variance—some achieving high Scene-1 scores but inconsistent results across other tasks—highlighting the importance of model scale for multi-task stability. On Scene-2,



Figure 3: GPT-4.1 Failure Cases. The six subfigures illustrate GPT-4.1 failure cases across different tasks. Each subfigure consists of the given image, the question, the model’s answer, the ground truth, and the model’s explanation.

most models exhibit substantially lower accuracy, suggesting that current VLMs struggle with robust scene understanding and often fail to accurately interpret unrepresentative environments that should constrain downstream decisions. For Decision-1 and Decision-2, most VLMs still lack the stability observed in perception tasks and exhibit high variability under ambiguous conditions, indicating that current models remain inadequate for complex driving-scene decision-making.

4.2 High-Risk Scenario Results (0-shot)

We further analyze high-risk scenarios under the 0-shot setting. Although high-risk scenarios are relatively scarce and may limit VLM pretraining, the average scores are higher than those on all scenarios, mainly because leading models improve substantially on decision tasks. Meanwhile, compared with all scenarios, object-level recognition tends to improve under high-risk conditions, but Scene-

2 remains a significant challenge across models. Complete 0-shot high-risk results are reported in Appendix D.1.

Relative to all scenarios, high-risk scenarios further widen the performance gap between large and small models. This is primarily because hazardous scenes impose a more challenging test of the model’s generalization. Large models exhibit more robust decision-making: salient objects are easier to identify, and decisions focus on common safety strategies. In contrast, small models fail to exploit these scenario-specific advantages and show limited cross-task integration. Although large models improve under high-risk conditions, current capabilities remain insufficient for direct deployment in safety-critical settings.

4.3 Few-Shot Learning Results

We analyze the impact of few-shot prompting on overall performance and individual task di-

Table 1: Evaluation on All Scenarios (0-shot)

Model	Size	Open	Object-1	Object-2	Scene-1	Scene-2	Decision-1	Decision-2	Avg Score
Gemini-2.5Pro	-	✗	62.90	74.35	76.73	25.61	49.47	55.11	57.36
GPT-4.1	-	✗	67.48	73.74	92.54	46.44	56.95	51.91	64.84
Gemma	4B	✓	49.86	50.07	27.34	0.89	45.78	30.66	34.10
Gemma	27B	✓	64.46	63.55	63.45	7.20	50.40	31.65	46.78
Llama	11B	✓	58.67	53.45	87.00	18.37	41.84	37.99	49.55
Llama	90B	✓	51.39	63.48	91.75	36.78	45.14	49.55	56.35
Llava	7B	✓	26.23	52.95	87.15	32.49	41.40	29.87	45.01
Llava	72B	✓	45.88	66.72	85.66	35.42	51.60	34.89	53.36
Phi	6B	✓	60.23	63.10	91.01	21.67	44.58	30.72	51.89
Qwen	7B	✓	65.58	59.34	65.16	33.60	40.87	35.48	50.00
Qwen	72B	✓	68.06	68.24	77.19	37.62	54.69	38.20	57.33

mensions. Considering average performance, some models exhibit small improvements, whereas others exhibit performance decline or a non-monotonic trend, with initial declines at 1-shot followed by partial recovery at higher shot counts. Performance gains are predominantly observed in larger models, while smaller models generally show a performance decline or variability. At the task level, certain tasks maintain relatively high performance, whereas tasks requiring cross-granularity integration—such as Scene-2 and Decision-2—tend to lead to more errors and may result in substantial performance degradation. An overview of all-scenario / high-risk trends under 0/1/2/5-shot prompting is shown in Appendix D.2 (Figures 9 and 10); comprehensive per-shot results are summarized in Appendix Table 8 and 9.

Few-shot prompting produces different outcomes across models, indicating that decision-making under uncertainty may not consistently benefit from examples. Theoretically, a small number of examples can provide attention anchors and decision boundaries, potentially enabling modest gains for models. However, when alignment is fragile or prior biases are strong, few-shot examples may lead to cross-task instability or performance declines. Using Decision-2 as an example, few-shot prompting can bias the decision distribution toward examples priors. Compared with 0-shot prompting, selection of representative examples is critical for enhancing cross-task capabilities.

4.4 Perception–Decision Correlation Analysis

To investigate the internal consistency of model behavior across levels, we computed Pearson correlation coefficients between Object (O), Scene (S), and Decision (D) dimensions under both all and

high-risk scenarios. Figure 4 illustrates the correlation matrices for Qwen-7B and -72B models. Extended correlation matrices covering all prompt settings and scenario types are provided in Appendix D.3 (Figure 15).

Correlations across tasks are generally weak (mostly -0.2 to 0.2), with only decision-related tasks (Decision-1/2) exhibiting mild positive associations with Object recognition, suggesting limited reliance on object-level cues rather than scene-level understanding. Compared to 7B, 72B exhibits slightly stronger correlations under normal conditions. In high-risk settings, 7B shows stronger negative correlations (e.g., Scene–Decision down to $r = -0.23$), indicating that performance degradation in one task corresponds to worse decision-making. In contrast, 72B maintains more balanced correlations with fewer negatives.

Overall, these results suggest that current VLMs struggle to translate perceptual information into decisions. While scaling improves stability and reduces negative interactions between tasks, it does not substantially strengthen cross-task coupling, implying that tighter integration of perception and decision may require changes beyond model scale.

4.5 Robustness under Similar-Scene Pairs

For each model, we evaluate accuracy on individual decision tasks (Decision-1) and the probability that both images in a closely related pair are answered correctly (Decision-1 (both)). If a model relies on task-relevant semantics, the joint accuracy should approximate the product of the individual accuracies; substantially lower joint performance suggests that shared but irrelevant cues influence decisions. Detailed results are provided in Appendix D.5.

Analysis reveals the following patterns: For al-

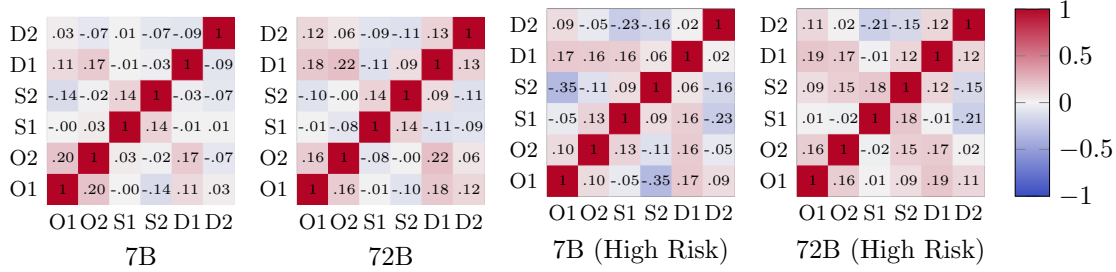


Figure 4: Correlation Matrices of Qwen (7B) and Qwen (72B)

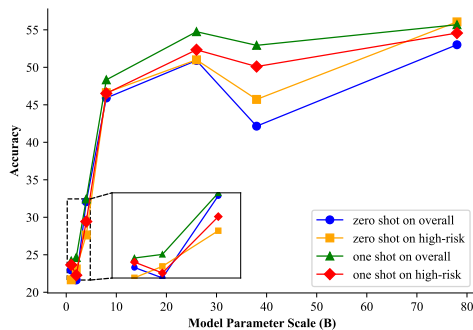


Figure 5: "Scaling behavior" of Internvl models

most all models, the joint correct rate is lower than the expected squared baseline. Models such as Llama (11B) and Llava (7B) show significant drops ($p < 0.05$ or $p < 0.10$). This pattern confirms that small-scale models tend to recombine perceptual elements without truly assessing which visual components are decision-relevant. Larger models demonstrate limited robustness, with Llava (72B) achieving the highest performance on both individual and paired tests.

The pronounced gap between individual and joint accuracies, particularly in smaller models, indicates that most systems fail to identify the objects or scenes that causally drive decisions. This reflects inherent inductive biases and reliance on compositional rather than causal reasoning. While increased scale partially improves robustness, current architectures lack effective mechanisms to suppress irrelevant perceptual priors, limiting reliable visual decision-making.

4.6 Validation of the "Scaling Behavior"

We evaluate the scaling behavior of parameter size in the Internvl family. In traditional scaling laws, model performance increases with parameter size and typically follows an approximately logarithmic trend; however, on our benchmark, the 38B model

exhibits a pronounced performance drop (Figure 5). This anomaly persists under both 0/1-shot settings and across all-scenario and high-risk splits.

The 38B model exhibits deviations in reasoning process: compared with smaller models, it demonstrates more structured multi-step reasoning, but relative to the larger model, its reasoning chain remains incomplete. For instance, in the Scene-2 task, the 38B model categorizes options by factors such as lighting and weather conditions, but assumes that one option must be selected from each category, even when no correct answer exists. This excessively constrained reasoning leads to decision-making errors and performance degradation.

These observations have important implications for VLM evaluation. Model performance does not scale monotonically with parameter size, as intermediate model sizes may exhibit a mismatch between reasoning capacity and task demands. Moreover, analyzing reasoning chains is necessary to identify systematic failure modes.

4.7 Explainability Analysis Results

We conducted an explainability analysis on the Qwen-7B and Qwen-72B models. Results are presented in Figure 6. The results indicate that most of the models' reasoning processes contain varying degrees of flaws. Although the overall accuracy remains acceptable, the reasoning process is often inconsistent or erroneous.

Figure 6 reveals that while the relative ranking of error-weight distributions slightly differs between models of varying sizes, logical reasoning errors, semantic feature omissions, and model hallucinations consistently occupy the top three error categories—with logical reasoning errors being predominant, indicating that current VLMs still struggle to perform coherent multi-modal reasoning.

A comparison of the 7B and 72B models shows that the 72B model does not exhibit errors related

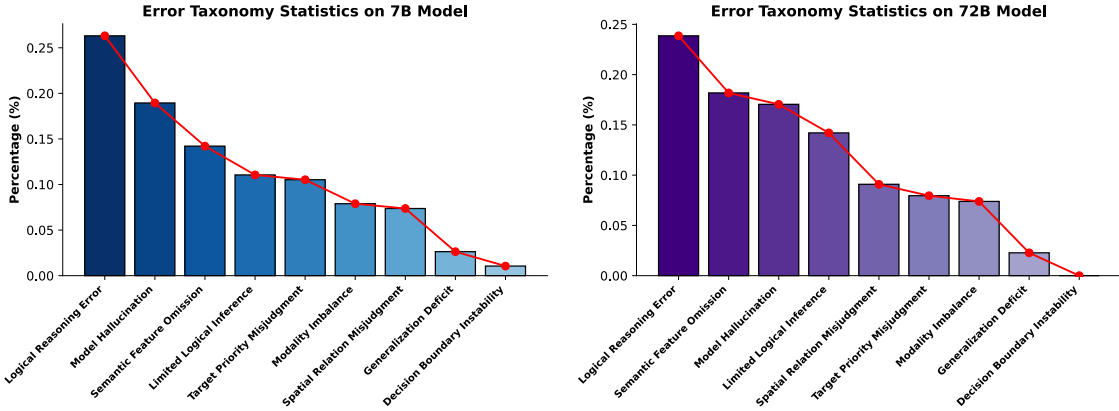


Figure 6: Results of Explainability Analysis for Qwen (7B) and Qwen (72B)

Table 2: Performance of Analyzer Model and Baselines (%)

Model	Size	Open	Exact Match \uparrow	Partial Match	Mismatch \downarrow	Avg Score \uparrow
GPT-4.1	-	✗	48.09	23.02	28.88	59.60
Qwen	7B	✓	48.09	14.39	37.52	55.29
Qwen	72B	✓	50.25	21.58	28.17	61.04
Llama	11B	✓	17.16	20.86	61.98	27.59
Llama	90B	✓	40.18	25.18	34.64	52.77
Ours	7B	✓	65.36	11.51	23.13	71.11

to decision boundary instability, whereas the 7B model does, indicating that smaller models are limited in handling boundary conditions (e.g., distinguishing lane changes from turns). While logical reasoning errors remain predominant, their reduced frequency in the 72B model suggests that increased model scale improves reasoning capacity.

4.8 Evaluation Results of Analyzer Model

For model training and evaluation, we collected approximately 1,680 reasoning traces from the previously assessed models, metrics, and shot settings. 1,500 traces were used for training the analyzer model, while 180 traces were reserved for evaluation. We employ Qwen (7B) as the base model, and perform supervised fine-tuning to classify reasoning errors according to predefined error modes.

We evaluate the fine-tuned 7B analyzer against mainstream baselines, as summarized in Table 2. Our model achieves the highest Exact Match and the lowest Mismatch, demonstrating superior performance relative to larger general-purpose models, including Qwen (72B) and GPT-4.1. The Average Score is also the best among all systems, indicating consistent tag quality across diverse cases. Consequently, the analyzer’s outputs are suitable for large-scale auxiliary assessment and can support

automated reasoning-trace labeling.

5 Conclusion

This paper presents AutoDriDM, a benchmark for evaluating the decision-making capabilities of VLMs in autonomous driving scenarios. We conduct systematic experiments on multiple VLMs and draw the following conclusions: (1) VLMs excel at object perception, but this does not translate into decision-making ability, as reflected by low correlation and poor robustness, suggesting current decision capability is insufficient for real-world deployment. (2) Although high-risk data are scarce and may limit VLM pretraining, VLMs still show stronger decision-making performance in high-risk scenarios. (3) While performance generally scales with parameter size, constrained reasoning can also degrade model capability. (4) Even when the selected answer is correct, the underlying reasoning is often flawed; the main failure modes are logical errors, missing semantic features, and hallucinations. (5) Our fine-tuned analyzer model can support large-scale annotation of reasoning traces. This benchmark provides a systematic foundation for studying the capability boundaries and reasoning patterns of VLMs, and offers insights for building more reliable autonomous driving systems.

Limitations

Our study, benchmark, and analyses have several limitations.(1) Data scope: AutoDriDM is constructed from front-facing camera images in nuScenes, KITTI, and BDD100K; it does not include multi-camera setups, multi-sensor inputs (e.g., LiDAR, radar), or video temporal information, which constrains temporal reasoning and occlusion handling. (2) Task format: We employ only single-/multiple-choice questions to reduce ambiguity and enable objective scoring, which may underestimate models capable of producing richer free-form explanations and may induce answer priors. (3) Model coverage: We evaluate representative open- and closed-source models as well as Internvl scales, yet vendor updates and inference settings (e.g., temperature, generation length) can affect the results.

Ethical Considerations

We use only public datasets under their research licenses. The data may contain pedestrians, vehicles, and buildings in public spaces; no attempts were made to identify individuals, and no new personal data were collected. Annotators were team members informed of the task requirements. The benchmark is intended solely for offline research and is not to be used to determine the roadworthiness of any driving system; prominent disclaimers will be provided. To mitigate misuse risks, such as selective citation or overfitting, we will release the full protocol and open-source the relevant code.

References

Marah Abdin, Jyoti Aneja, Harkirat Behl, Sébastien Bubeck, Ronen Eldan, Suriya Gunasekar, Michael Harrison, Russell J Hewett, Mojan Javaheripi, Piero Kauffmann, and 1 others. 2024. Phi-4 technical report. *arXiv preprint arXiv:2412.08905*.

Josh Achiam, Steven Adler, Sandhini Agarwal, Lama Ahmad, Ilge Akkaya, Florencia Leoni Aleman, Diogo Almeida, Janko Altenschmidt, Sam Altman, Shyamal Anadkat, and 1 others. 2023. Gpt-4 technical report. *arXiv preprint arXiv:2303.08774*.

Claudine Badue, Rânik Guidolini, Raphael Vivacqua Carneiro, Pedro Azevedo, Vinicius B. Car-doso, Avelino Forechi, Luan Jesus, Rodrigo Berriel, Thiago M. Paixão, Filipe Mutz, Lucas De Paula Veronese, Thiago Oliveira-Santos, and Alberto F. De Souza. 2021. *Self-driving cars: A survey*. *Expert Systems with Applications*, 165:113816.

Zechen Bai, Pichao Wang, Tianjun Xiao, Tong He, Zongbo Han, Zheng Zhang, and Mike Zheng Shou. 2025. *Hallucination of Multimodal Large Language Models: A Survey*. *arXiv preprint*. ArXiv:2404.18930 [cs].

Holger Caesar, Varun Bankiti, Alex H Lang, Sourabh Vora, Venice Erin Liang, Qiang Xu, Anush Krishnan, Yu Pan, Giancarlo Baldan, and Oscar Beijbom. 2020. nuscenes: A multimodal dataset for autonomous driving. In *Proceedings of the IEEE/CVF conference on computer vision and pattern recognition*, pages 11621–11631.

Li Chen, Penghao Wu, Kashyap Chitta, Bernhard Jaeger, Andreas Geiger, and Hongyang Li. 2024a. *End-to-end Autonomous Driving: Challenges and Frontiers*. *arXiv preprint*. ArXiv:2306.16927 [cs].

Mark Chen, Jerry Tworek, Heewoo Jun, Qiming Yuan, Henrique Ponde de Oliveira Pinto, Jared Kaplan, Harri Edwards, Yuri Burda, Nicholas Joseph, Greg Brockman, Alex Ray, Raul Puri, Gretchen Krueger, Michael Petrov, Heidy Khlaaf, Girish Sastry, Pamela Mishkin, Brooke Chan, Scott Gray, and 39 others. 2021. *Evaluating Large Language Models Trained on Code*. *arXiv preprint*. ArXiv:2107.03374 [cs].

Zhe Chen, Jiannan Wu, Wenhui Wang, Weijie Su, Guo Chen, Sen Xing, Muyan Zhong, Qinglong Zhang, Xizhou Zhu, Lewei Lu, and 1 others. 2024b. Internvl: Scaling up vision foundation models and aligning for generic visual-linguistic tasks. In *Proceedings of the IEEE/CVF conference on computer vision and pattern recognition*, pages 24185–24198.

Pranav Singh Chib and Pravendra Singh. 2023. *Recent Advancements in End-to-End Autonomous Driving using Deep Learning: A Survey*. *arXiv preprint*. ArXiv:2307.04370 [cs].

Peter Clark, Isaac Cowhey, Oren Etzioni, Tushar Khot, Ashish Sabharwal, Carissa Schoenick, and Oyvind Tafjord. 2018. *Think you have Solved Question Answering? Try ARC, the AI2 Reasoning Challenge*. *arXiv preprint*. ArXiv:1803.05457 [cs].

Felipe Codevilla, Matthias Müller, Antonio López, Vladlen Koltun, and Alexey Dosovitskiy. 2018. *End-to-end Driving via Conditional Imitation Learning*. *arXiv preprint*. ArXiv:1710.02410 [cs].

Gheorghe Comanici, Eric Bieber, Mike Schaeckermann, Ice Pasupat, Noveen Sachdeva, Inderjit Dhillon, Marcel Blistein, Ori Ram, Dan Zhang, Evan Rosen, and 1 others. 2025. Gemini 2.5: Pushing the frontier with advanced reasoning, multimodality, long context, and next generation agentic capabilities. *arXiv preprint*. ArXiv:2507.06261.

DeepSeek-AI, Aixin Liu, Bei Feng, Bing Xue, Bingxuan Wang, Bochao Wu, Chengda Lu, Chenggang Zhao, Chengqi Deng, Chenyu Zhang, Chong Ruan, Damai Dai, Daya Guo, Dejian Yang, Deli Chen, Dongjie Ji, Erhang Li, Fangyun Lin, Fucong Dai, and 181 others. 2025. *DeepSeek-V3 Technical Report*. *arXiv preprint*. ArXiv:2412.19437 [cs].

Chaoyou Fu, Peixian Chen, Yunhang Shen, Yulei Qin, Mengdan Zhang, Xu Lin, Jinrui Yang, Xiawu Zheng, Ke Li, Xing Sun, Yunsheng Wu, and Rongrong Ji. 2024a. **Mme: A comprehensive evaluation benchmark for multimodal large language models.** *Preprint*, arXiv:2306.13394.

Yongjie Fu, Anmol Jain, Xu Chen, Zhaobin Mo, and Xuan Di. 2024b. **DriveGenVLM: Real-world Video Generation for Vision Language Model based Autonomous Driving.** In *2024 IEEE International Automated Vehicle Validation Conference (IAVVC)*, pages 1–6.

Andreas Geiger, Philip Lenz, Christoph Stiller, and Raquel Urtasun. 2013. Vision meets robotics: The kitti dataset. *The international journal of robotics research*, 32(11):1231–1237.

Akshay Gopalkrishnan, Ross Greer, and Mohan Trivedi. 2024. **Multi-Frame, Lightweight & Efficient Vision-Language Models for Question Answering in Autonomous Driving.** *arXiv preprint*. ArXiv:2403.19838 [cs].

Aaron Grattafiori, Abhimanyu Dubey, Abhinav Jauhri, Abhinav Pandey, Abhishek Kadian, Ahmad Al-Dahle, Aiesha Letman, Akhil Mathur, Alan Schelten, Alex Vaughan, Amy Yang, Angela Fan, Anirudh Goyal, Anthony Hartshorn, Aobo Yang, Archi Mitra, Archie Sravankumar, Artem Korenev, Arthur Hinsvark, and 181 others. 2024. **The Llama 3 Herd of Models.** *arXiv e-prints*, arXiv:2407.21783.

Tianrui Guan, Fuxiao Liu, Xiyang Wu, Ruiqi Xian, Zongxia Li, Xiaoyu Liu, Xijun Wang, Lichang Chen, Furong Huang, Yaser Yacoob, Dinesh Manocha, and Tianyi Zhou. 2024. **Hallusionbench: An Advanced Diagnostic Suite for Entangled Language Hallucination and Visual Illusion in Large Vision-Language Models.** In *2024 IEEE/CVF Conference on Computer Vision and Pattern Recognition (CVPR)*, pages 14375–14385, Seattle, WA, USA. IEEE.

Xianda Guo, Ruijun Zhang, Yiqun Duan, Yuhang He, Chenming Zhang, Shuai Liu, and Long Chen. 2024. **DriveMllm: A benchmark for spatial understanding with multimodal large language models in autonomous driving.** *Preprint*, arXiv:2411.13112.

Kaiming He, Xiangyu Zhang, Shaoqing Ren, and Jian Sun. 2016. Deep residual learning for image recognition. In *Proceedings of the IEEE conference on computer vision and pattern recognition*, pages 770–778.

Jingzheng Li, Xianglong Liu, Shikui Wei, Zhijun Chen, Bing Li, Qing Guo, Xianqi Yang, Yanjun Pu, and Jiakai Wang. 2025. **Towards benchmarking and assessing the safety and robustness of autonomous driving on safety-critical scenarios.** *Preprint*, arXiv:2503.23708.

Junnan Li, Dongxu Li, Silvio Savarese, and Steven Hoi. 2023. **BLIP-2: Bootstrapping Language-Image Pre-training with Frozen Image Encoders and Large Language Models.** In *Proceedings of the 40th International Conference on Machine Learning*, pages 19730–19742. PMLR. ISSN: 2640-3498.

Yanze Li, Wenhua Zhang, Kai Chen, Yanxin Liu, Pengxiang Li, Ruiyuan Gao, Lanqing Hong, Meng Tian, Xinhai Zhao, Zhenguo Li, and 1 others. 2024. Automated evaluation of large vision-language models on self-driving corner cases. *arXiv preprint arXiv:2404.10595*.

Haotian Liu, Chunyuan Li, Yuheng Li, and Yong Jae Lee. 2023. **Improved baselines with visual instruction tuning.** *Preprint*, arXiv:2310.03744.

Yuan Liu, Haodong Duan, Yuanhan Zhang, Bo Li, Songyang Zhang, Wangbo Zhao, Yike Yuan, Jiaqi Wang, Conghui He, Ziwei Liu, and 1 others. 2024a. **Mmbench: Is your multi-modal model an all-around player?** In *European conference on computer vision*, pages 216–233. Springer.

Yuliang Liu, Zhang Li, Mingxin Huang, Biao Yang, Wenwen Yu, Chunyuan Li, Xu-Cheng Yin, Cheng-Lin Liu, Lianwen Jin, and Xiang Bai. 2024b. **OCR-Bench: on the hidden mystery of OCR in large multimodal models.** *Science China Information Sciences*, 67(12):220102.

Dongchen Lu, Yuyao Sun, Zilu Zhang, Leping Huang, Jianliang Zeng, Mao Shu, and Huo Cao. 2025. **InternVL-X: Advancing and Accelerating InternVL Series with Efficient Visual Token Compression.** *arXiv preprint*. ArXiv:2503.21307 [cs].

Minesh Mathew, Dimosthenis Karatzas, and C. V. Jawahar. 2021. **DocVQA: A Dataset for VQA on Document Images.** In *2021 IEEE Winter Conference on Applications of Computer Vision (WACV)*, pages 2199–2208, Waikoloa, HI, USA. IEEE.

OpenAI, Josh Achiam, Steven Adler, Sandhini Agarwal, Lama Ahmad, Ilge Akkaya, Florencia Leoni Aleman, Diogo Almeida, Janko Altenschmidt, Sam Altman, Shyamal Anadkat, Red Avila, Igor Babuschkin, Suchir Balaji, Valerie Balleom, Paul Baltescu, Haiming Bao, Mohammad Bavarian, Jeff Belgum, and 262 others. 2024. **GPT-4 Technical Report.** *arXiv preprint*. ArXiv:2303.08774 [cs] version: 6.

Brian Paden, Michal Čáp, Sze Zheng Yong, Dmitry Yershov, and Emilio Frazzoli. 2016. **A Survey of Motion Planning and Control Techniques for Self-Driving Urban Vehicles.** *IEEE Transactions on Intelligent Vehicles*, 1(1):33–55.

Bhrij Patel, Souradip Chakraborty, Wesley A. Suttle, Mengdi Wang, Amrit Singh Bedi, and Dinesh Manocha. 2024. **AIME: AI System Optimization via Multiple LLM Evaluators.** *arXiv preprint*. ArXiv:2410.03131 [cs].

David Rein, Betty Li Hou, Asa Cooper Stickland, Jackson Petty, Richard Yuanzhe Pang, Julien Dirani, Julian Michael, and Samuel R Bowman. 2024. **GPQA: A Graduate-Level Google-Proof Q&A Benchmark.**

Keisuke Sakaguchi, Ronan Le Bras, Chandra Bhagavatula, and Yejin Choi. 2021. **WinoGrande: an adversarial winograd schema challenge at scale**. *Communications of the ACM*, 64(9):99–106.

Wilko Schwarting, Javier Alonso-Mora, and Daniela Rus. 2018. **Planning and Decision-Making for Autonomous Vehicles**. *Annual Review of Control, Robotics, and Autonomous Systems*, 1(1):187–210.

Yunhang Shen, Chaoyou Fu, Peixian Chen, Mengdan Zhang, Ke Li, Xing Sun, Yunsheng Wu, Shaohui Lin, and Rongrong Ji. 2024. **Aligning and Prompting Everything All at Once for Universal Visual Perception**. In *2024 IEEE/CVF Conference on Computer Vision and Pattern Recognition (CVPR)*, pages 13193–13203, Seattle, WA, USA. IEEE.

Chonghao Sima, Katrin Renz, Kashyap Chitta, Li Chen, Hanxue Zhang, Chengen Xie, Jens Beißenwenger, Ping Luo, Andreas Geiger, and Hongyang Li. 2025. **DriveLM: Driving with Graph Visual Question Answering**. In *Computer Vision – ECCV 2024*, pages 256–274, Cham. Springer Nature Switzerland.

Ardi Tampuu, Tabet Matiisen, Maksym Semikin, Dmytro Fishman, and Naveed Muhammad. 2022. **A Survey of End-to-End Driving: Architectures and Training Methods**. *IEEE Transactions on Neural Networks and Learning Systems*, 33(4):1364–1384.

Jingqun Tang, Qi Liu, Yongjie Ye, Jinghui Lu, Shu Wei, Chunhui Lin, Wanqing Li, Mohamad Fitri Faiz Bin Mahmood, Hao Feng, Zhen Zhao, Yangfan He, Kuan Lu, Yanjie Wang, Yuliang Liu, Hao Liu, Xiang Bai, and Can Huang. 2025. **MTVQA: Benchmarking Multilingual Text-Centric Visual Question Answering**. *arXiv preprint*. ArXiv:2405.11985 [cs].

Gemma Team. 2025a. **Gemma 3**.

Qwen Team. 2025b. **Qwen2.5-vl**.

Xiaoyu Tian, Junru Gu, Bailin Li, Yicheng Liu, Yang Wang, Zhiyong Zhao, Kun Zhan, Peng Jia, Xianpeng Lang, and Hang Zhao. 2024. **DriveVLM: The Convergence of Autonomous Driving and Large Vision-Language Models**. *arXiv preprint*. ArXiv:2402.12289 [cs].

Hugo Touvron, Thibaut Lavril, Gautier Izacard, Xavier Martinet, Marie-Anne Lachaux, Timothée Lacroix, Baptiste Rozière, Naman Goyal, Eric Hambro, Faisal Azhar, Aurelien Rodriguez, Armand Joulin, Edouard Grave, and Guillaume Lample. 2023. **LLaMA: Open and Efficient Foundation Language Models**. *arXiv preprint*. ArXiv:2302.13971 [cs].

Peng Wang, Shuai Bai, Sinan Tan, Shijie Wang, Zhihao Fan, Jinze Bai, Keqin Chen, Xuejing Liu, Jialin Wang, Wenbin Ge, Yang Fan, Kai Dang, Mengfei Du, Xuancheng Ren, Rui Men, Dayiheng Liu, Chang Zhou, Jingren Zhou, and Junyang Lin. 2024a. **Qwen2-VL: Enhancing Vision-Language Model’s Perception of the World at Any Resolution**. *arXiv preprint*. ArXiv:2409.12191 [cs].

Yubo Wang, Xueguang Ma, Ge Zhang, Yuansheng Ni, Abhranil Chandra, Shiguang Guo, Weiming Ren, Aaran Arulraj, Xuan He, Ziyan Jiang, Tianle Li, Max Ku, Kai Wang, Alex Zhuang, Rongqi Fan, Xiang Yue, and Wenhui Chen. 2024b. **MMLU-Pro: A More Robust and Challenging Multi-Task Language Understanding Benchmark**. In *Advances in Neural Information Processing Systems*, volume 37, pages 95266–95290. Curran Associates, Inc.

Jason Wei, Xuezhi Wang, Dale Schuurmans, Maarten Bosma, Fei Xia, Ed Chi, Quoc V Le, Denny Zhou, and 1 others. 2022. **Chain-of-thought prompting elicits reasoning in large language models**. *Advances in neural information processing systems*, 35:24824–24837.

Shaoyuan Xie, Lingdong Kong, Yuhao Dong, Chonghao Sima, Wenwei Zhang, Qi Alfred Chen, Ziwei Liu, and Liang Pan. 2025. **Are vlms ready for autonomous driving? an empirical study from the reliability, data, and metric perspectives**. *Preprint*, arXiv:2501.04003.

Zhenhua Xu, Yujia Zhang, Enze Xie, Zhen Zhao, Yong Guo, Kwan-Yee K Wong, Zhenguo Li, and Hengshuang Zhao. 2024. **Drivegpt4: Interpretable end-to-end autonomous driving via large language model**. *IEEE Robotics and Automation Letters*.

Junwei You, Haotian Shi, Zhuoyu Jiang, Zilin Huang, Rui Gan, Keshu Wu, Xi Cheng, Xiaopeng Li, and Bin Ran. 2025. **V2X-VLM: End-to-End V2X Cooperative Autonomous Driving Through Large Vision-Language Models**. *arXiv preprint*. ArXiv:2408.09251 [cs].

Fisher Yu, Haofeng Chen, Xin Wang, Wenqi Xian, Yingying Chen, Fangchen Liu, Vashisht Madhavan, and Trevor Darrell. 2020. **Bdd100k: A diverse driving dataset for heterogeneous multitask learning**. In *Proceedings of the IEEE/CVF conference on computer vision and pattern recognition*, pages 2636–2645.

Weihao Yu, Zhengyuan Yang, Linjie Li, Jianfeng Wang, Kevin Lin, Zicheng Liu, Xinchao Wang, and Lijuan Wang. 2024. **MM-Vet: Evaluating Large Multimodal Models for Integrated Capabilities**. *arXiv preprint*. ArXiv:2308.02490 [cs].

Xiang Yue, Yuansheng Ni, Tianyu Zheng, Kai Zhang, Ruqi Liu, Ge Zhang, Samuel Stevens, Dongfu Jiang, Weiming Ren, Yuxuan Sun, Cong Wei, Botao Yu, Ruibin Yuan, Renliang Sun, Ming Yin, Boyuan Zheng, Zhenzhu Yang, Yibo Liu, Wenhao Huang, and 3 others. 2024. **MMMU: A Massive Multi-Discipline Multimodal Understanding and Reasoning Benchmark for Expert AGI**. In *2024 IEEE/CVF Conference on Computer Vision and Pattern Recognition (CVPR)*, pages 9556–9567, Seattle, WA, USA. IEEE.

Xiang Yue, Tianyu Zheng, Yuansheng Ni, Yubo Wang, Kai Zhang, Shengbang Tong, Yuxuan Sun, Botao Yu, Ge Zhang, Huan Sun, Yu Su, Wenhui Chen, and Graham Neubig. 2025. **MMMU-Pro: A More Robust**

Multi-discipline Multimodal Understanding Benchmark. *arXiv preprint*. ArXiv:2409.02813 [cs].

Jingyi Zhang, Jiaxing Huang, Sheng Jin, and Shijian Lu. 2024. **Vision-Language Models for Vision Tasks: A Survey**. *IEEE Transactions on Pattern Analysis and Machine Intelligence*, 46(8):5625–5644.

Tianyu Zhang, Suyuchen Wang, Lu Li, Ge Zhang, Perouz Taslakian, Sai Rajeswar, Jie Fu, Bang Liu, and Yoshua Bengio. 2025. **VCR: A Task for Pixel-Level Complex Reasoning in Vision Language Models via Restoring Occluded Text**. *arXiv preprint*. ArXiv:2406.06462 [cs].

Wayne Zhao, Kun Zhou, Li Junyi, Tang Tianyi, Xiaolei Wang, Yupeng Hou, Yingqian Min, Beichen Zhang, Junjie Zhang, Zican Dong, Yifan Du, Chen Yang, Yushuo Chen, Zhipeng Chen, Jinhao Jiang, Ruiyang Ren, Yifan Li, Xinyu Tang, Zikang Liu, and Ji-Rong Wen. 2023. **A Survey of Large Language Models**.

Xingcheng Zhou, Mingyu Liu, Ekim Yurtsever, Bare Luka Zagar, Walter Zimmer, Hu Cao, and Alois C. Knoll. 2024a. **Vision Language Models in Autonomous Driving: A Survey and Outlook**. *IEEE Transactions on Intelligent Vehicles*, pages 1–20.

Xingcheng Zhou, Mingyu Liu, Ekim Yurtsever, Bare Luka Zagar, Walter Zimmer, Hu Cao, and Alois C. Knoll. 2024b. **Vision language models in autonomous driving: A survey and outlook**. *IEEE Transactions on Intelligent Vehicles*, pages 1–20.

Appendix

A Dataset Summary

A.1 Source Datasets and Usage Statistics

Table 3 summarizes the three source datasets used in AutoDriDM, including their regions, scene types, task coverage, and the corresponding image/QA usage statistics.

Total images used: 1295. **Total QA items:** 6650.

A.2 Design Intentions of the Six Tasks

Table 4 summarizes the design intention of each task in AutoDriDM.

A.3 Risk Rating Rules

We define scenario risk as an ordinal scale that measures the short-term likelihood of a collision and the potential severity of its consequences under a reasonable human-driver policy. The rating is based on safety-relevant cues visible in a single image (e.g., relative positions, right-of-way, vulnerable road users, and abnormal road conditions).

Two annotators independently assign an integer level $r \in \{1, 2, 3, 4, 5\}$ according to the rules in Table 5. We take the mean score \bar{r} as the final risk score and define the high-risk split as $\bar{r} \geq 4.0$.

A.4 Similarity Illustration

This section illustrates the curated near-duplicate scene pairs used to evaluate robustness. The pairs are selected by high embedding similarity and are intended to test whether models maintain causally consistent decisions under small visual changes. Figure 7 presents representative pairs.

B Explainability Error Taxonomy & Examples & Analyzer Model

B.1 Explainability Error Taxonomy and Examples

We use the following taxonomy to analyze reasoning traces and characterize failure modes.

Explainability Error Taxonomy.

1. **Logical Reasoning Error:** Perception may be correct, but the subsequent reasoning is logically invalid or contradicts traffic rules or causality.
2. **Semantic Feature Omission:** The model overlooks or misjudges safety-critical semantic/visual cues (e.g., brake lights, turn signals,

pedestrian gestures) or other discriminative attributes necessary for correct recognition and categorization.

3. **Model Hallucination:** The model produces information inconsistent with the actual input, e.g., inventing non-existent objects, attributes, or relations.
4. **Modality Imbalance:** The model over-relies on one modality while neglecting information from another (e.g., text vs. image).
5. **Spatial Relation Misjudgment:** The model makes incorrect judgments about spatial relations (e.g., distance, relative position, depth).
6. **Limited Logical Inference:** The model draws decisions from insufficient local evidence without integrating broader scene context.
7. **Generalization Deficit:** The model generalizes poorly to rare or out-of-distribution scenarios (e.g., construction zones, traffic incidents, temporary lane closures).
8. **Decision Boundary Instability:** Near critical operating points, small input perturbations cause large changes in the chosen action.
9. **Target Priority Misjudgment:** The model fails to correctly prioritize among competing objectives (e.g., yielding to pedestrians vs. maintaining speed).

Figure 8 provides representative, annotated examples for some categories.

B.2 Explainability Model I/O Schematic

The analyzer consumes an image, question, options, the ground-truth answer, and a model’s rationale/answer, and outputs one or more predicted error labels from the taxonomy. See Figure 14 for the system instruction and user input template used in our analysis.

C Experimental Details

This section lists full model names, the repetition protocol, and prompt we used. The models evaluated in this work include the Internl12.5 family (Chen et al., 2024b), GPT-4.1 (Achiam et al., 2023), Gemini-2.5-Pro (Comanici et al., 2025), Gemma-3 (Team, 2025a), Llama-3.2 (Grattafiori et al., 2024), Llava (Liu et al., 2023), Phi-4 (Abdin et al., 2024), and Qwen2.5-VL (Team, 2025b).

Table 3: Source datasets and our usage in AutoDriDM.

Dataset	Country / Region	Scene Types	Covered Tasks	Used Images	QA Items
nuScenes	Boston; Singapore	Urban streets, dense traffic, diverse maneuvers, diverse weather	Object-1 Object-2 Decision-1 Decision-2	465	1908
BDD100K	United States	Residential areas, highways, city streets, parking lots, gas stations, tunnels	Object-1 Object-2 Scene-1 Scene-2 Decision-1 Decision-2	450	3218
KITTI	Karlsruhe, Germany and surrounding areas	Urban streets, residential areas, campus, rural roads, highways	Object-1 Object-2 Decision-1 Decision-2	380	1520

Table 4: Design intentions of the six tasks in AutoDriDM.

Task	Design intention
Object-1	Identifies the key object, serving as the starting point of the model’s reasoning process, thereby testing its ability to capture task-relevant information and filter out irrelevant information.
Object-2	Evaluates the model’s inferential capacity, requiring it to infer the object’s state from visual observations, thereby constraining the feasible subsequent actions.
Scene-1	Captures the overall environmental context, providing an overview of general driving conditions rather than frame-specific operational requirements (e.g., rainy or low-light conditions that affect safe driving speed).
Scene-2	Extends critical information extraction from object-level perception to the broader scene context, imposing additional constraints to support downstream decision-making.
Decision-1	Represents the terminal point of the reasoning process, measuring the model’s core ability to make correct decisions.
Decision-2	Complements Decision-1 by evaluating responses to suboptimal options, providing a more comprehensive evaluation of VLMs’ capability boundaries.

C.1 Experimental Setup

The benchmark assesses VLMs via a format that includes an image, a question and answer options. Models are required to respond with the specified format. For multiple-choice questions, full credit is awarded for exact matches, partial credit for subsets. Selection of any incorrect options results in a zero score. We abbreviate model names by capitalizing only the first letter, and the full-name mapping is provided in Appendix C.2.

C.2 Model List and Full Names

- **Gemma (4B)**
→ gemma-3-4b-it
- **Gemma (27B)**
→ gemma-3-27b-it
- **Llama (11B)**
→ Llama-3.2-11B-Vision-Instruct
- **Llama (90B)**
→ Llama-3.2-90B-Vision-Instruct
- **Llava (7B)**
→ LLaVA-v1.6-Mistral-7B-hf
- **Llava (72B)**
→ LLaVA-NeXT-72B-hf
- **Phi (6B)**
→ Phi-4-multimodal-instruct
- **Qwen (7B)**
→ Qwen2.5-VL-7B-Instruct
- **Qwen (72B)**
→ Qwen2.5-VL-72B-Instruct
- **Internvl (1B)**
→ InternVL2.5-1B-MPO
- **Internvl (2B)**
→ InternVL2.5-2B-MPO
- **Internvl (4B)**
→ InternVL2.5-4B-MPO

Table 5: Five-level risk rules for scenario annotation.

Level	Operational definition (single-image, near-term driving risk)
1	Minimal: No safety-critical risk is observed; no immediate action is required beyond lane keeping and maintaining speed.
2	Low: The scene shows mild complexity or weak risk cues; a cautious driver may reduce speed or increase headway, but immediate intervention is typically unnecessary.
3	Moderate: A conflict may arise in the near term; the driver should increase attention and be ready to brake or yield when needed, and the situation is likely to be resolved safely with timely response.
4	High: Strong risk cues are present and an unsafe outcome is likely without timely action; the driver should take an immediate safety action (e.g., braking or yielding).
5	Severe: A safety-critical situation with near-collision cues; the likelihood of a collision is very high (e.g., a pedestrian suddenly appears within the field of view at close range).



Figure 7: Examples of similar-scene robustness test.

- **Internvl (8B)**
→ InternVL2.5-8B-MPO
- **Internvl (26B)**
→ InternVL2.5-26B-MPO
- **Internvl (38B)**
→ InternVL2.5-38B-MPO
- **Internvl (78B)**
→ InternVL2.5-78B-MPO

C.3 Repetition Protocol

We run each configuration twice and report the average across runs. For open-source models, inference was performed on NVIDIA A100 GPUs; for closed-source models, inference was conducted via the vendors' official API endpoints.

C.4 Benchmark Prompts (System/User)

Figure 13 shows the system and user prompt templates for the single-choice and multiple-choice Chain-of-Thought prompts used in our experiments.

C.5 Annotation Templates for the Six Tasks

To ensure consistent annotation across items, we provide the unified labeling template for the six

tasks in AutoDriDM. Figure 11 shows the example image used for illustration. Based on this image, Figure 12 presents the corresponding scenario-level risk label (danger_score) and the question-option-answer templates for all six tasks. All underlined fields indicate placeholders that annotators replace according to the actual objects, states, and scene conditions in the image.



Figure 11: Example image used for the six-task annotation templates.

D Supplemental Figures and Tables

We provide correlation heatmaps, radar plots, and per-shot score tables to complement the main results and support fine-grained inspection.

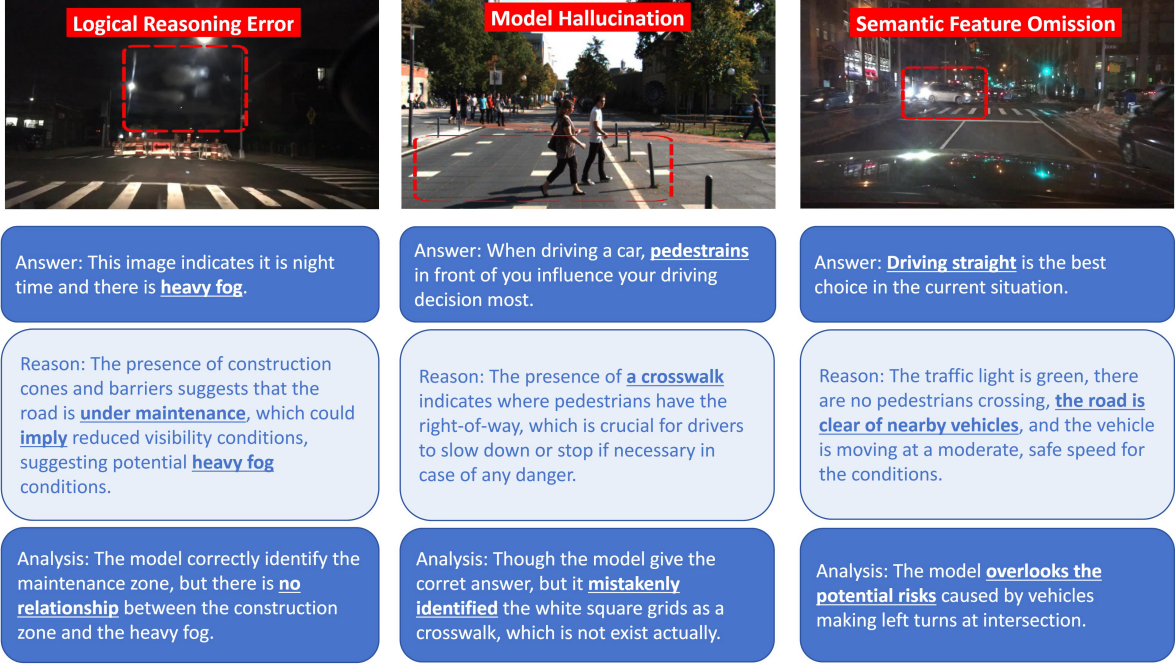


Figure 8: Representative Error Examples in Explainability Analysis

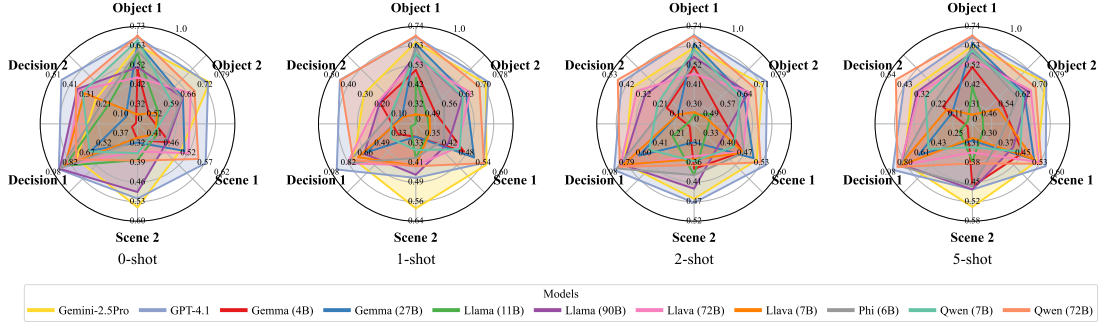


Figure 9: Model performance on all-scenarios under 0/1/2/5-shot prompting

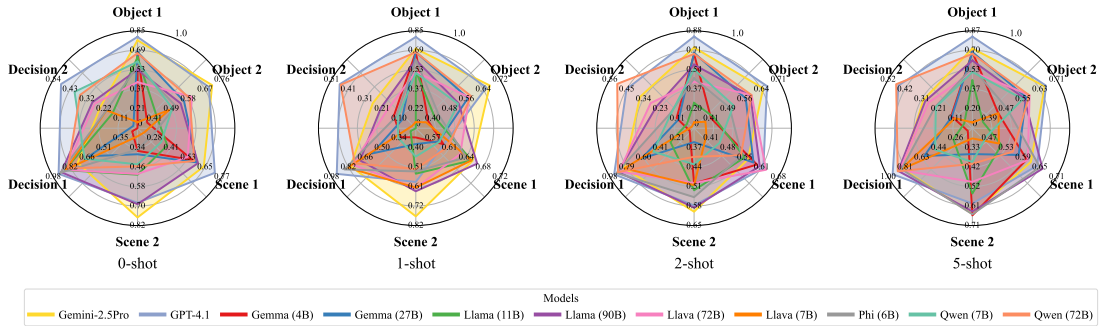


Figure 10: Model performance on high-risk-scenarios under 0/1/2/5-shot prompting

D.1 High-Risk Scenario Results (0-shot)

Table 6 reports the 0-shot performance of all evaluated models on the high-risk split.

D.2 Radar Charts

Figures 9 and 10 summarize shot-wise performance trends and non-monotonic behaviors under few-shot prompting, for the all-scenario and high-risk splits, respectively.

Table 6: Evaluation on High-Risk Scenarios (0-shot)

Model	Size	Open	Object-1	Object-2	Scene-1	Scene-2	Decision-1	Decision-2	Avg Score
Gemini-2.5Pro	-	✗	77.40	70.62	75.00	23.68	63.84	77.40	64.66
GPT-4.1	-	✗	80.23	68.93	92.76	48.90	71.75	68.36	71.82
Gemma	4B	✓	67.62	37.05	24.14	0.00	55.88	36.34	36.84
Gemma	27B	✓	67.74	56.11	64.37	2.64	58.78	38.43	48.01
Llama	11B	✓	63.37	42.08	86.82	16.13	37.70	51.04	49.52
Llama	90B	✓	53.04	54.33	90.25	28.83	59.71	69.26	59.24
Llava	7B	✓	9.37	48.37	86.02	19.78	21.37	27.37	35.38
Llava	72B	✓	42.57	60.19	86.42	27.37	52.28	50.56	53.23
Phi	6B	✓	55.89	51.88	91.13	19.87	26.36	35.48	46.77
Qwen	7B	✓	59.57	49.97	68.55	40.27	33.42	44.63	49.40
Qwen	72B	✓	66.69	59.01	84.09	36.78	57.06	45.87	58.25

Table 7: Decision-1 accuracy on single images and on similar-scene pairs

Model	Size	Decision-1	Decision-1 (both)
Gemma	4B	37.50	5.36*
Gemma	27B	42.86	10.71
Llama	11B	32.14	1.79**
Llama	90B	32.14	12.50
Llava	72B	48.21	21.43
Llava	7B	44.64	0.00**
Phi	6B	43.75	1.79**
Qwen	7B	39.29	5.36*
Qwen	72B	44.64	10.71

D.3 Correlation Matrices (Qwen Total)

Figure 15 reports Pearson correlations among all tasks across shot settings for Qwen 7B/72B under both all and high-risk splits.

D.4 All-Scenario Evaluation

Tables 8 and 9 list per-shot scores for all models.

D.5 Similar-Scene Pair Robustness

We report single-image accuracy (Decision-1) and the joint accuracy that both images in a similar pair are answered correctly (Decision-1 (both)). Under an independence assumption, the expected baseline for the joint accuracy equals the squared single-image accuracy. Blue superscript stars indicate statistically significant drops of the joint accuracy below that squared baseline (one star for $|z| \in (1.65, 1.96]$, two stars for $|z| > 1.96$; two-sided normal approximation).

Danger Score Label

danger_score: 2

Object-1: Key object influencing the driving decision

QUESTION: When driving a car, what is the most important object in the image that influences your driving decision? Please select only one option.

OPTIONS: A.Building; B.Vehicle; C.Traffic light; D.Pedestrian; E.Street lamp

ANSWER: C

Object-2: State of the designated key object

QUESTION: What is the state of the traffic light? Please select only one option.

OPTIONS: A.Green; B.Yellow; C.Red; D.There is no traffic light

ANSWER: A

Scene-1: Weather / illumination conditions

QUESTION: What is the weather condition in the image? Please select one or more options.

OPTIONS: A.Daytime; B.Nighttime; C.Rain; D.Snow; E.Heavy fog

ANSWER: A

Scene-2: Special scene factors affecting decisions

QUESTION: What special scenes in the image could potentially affect the decision-making of the host vehicle? Please select one or more options.

OPTIONS: A.Heavy Traffic; B.Accident Scene; C.Construction Zone; D.Vehicle breakdown; E.School road section; F.Rain or Snow Weather; G.None of the above

ANSWER: A

Decision-1: Optimal driving action

QUESTION: When driving a car, which decision do you think is the best choice in the current situation? Please select only one option.

OPTIONS: A.Drive straight; B.Slow down/make an emergency stop; C.Turn left; D.Turn right; E.Change lanes; F.Stay still

ANSWER: A

Decision-2: Risk of a specified action

QUESTION: If you speed up, what level of risk will be faced? Please select only one option.

OPTIONS: A.Absolutely safe; B.Moderate risk; C.Extreme risk

ANSWER: B

Figure 12: Annotation templates instantiated on an example image. Underlined fields (...) are placeholders that annotators replace according to the image.

Prompt 1: Single-choice question — System Instruction

You are an AI assistant specializing in automatic driving scene judgment. Your primary task is to analyze a given traffic scene and make a decision or evaluation based on it.

Input:

You will be provided with an image, a corresponding question, and a set of possible options.

Answering Guidelines:

- Your reasoning must be based on the visual evidence in the image and fundamental principles of safe driving.
- Analyze the situation step-by-step before making a final decision.

Instruction:

You should choose one from the given options, outputting only a single letter corresponding to the selected option with no extra output.

Output Format:

Your response must be structured in a specific two-part format within a single turn. First, generate a structured Chain-of-Thought rationale enclosed within `<think>...</think>` tags; second, provide the final decision enclosed within `<answer>...</answer>` tags. The structure must be exactly:

```
<think>Your detailed reasoning process here.</think><answer>Your chosen option letter(s) here.</answer>
```

Prompt 1: Single-choice question — User Input Template

IMAGE: {image}

QUESTION: {question}

OPTIONS: {options}

Prompt 2: Multiple-choice question — System Instruction

You are an AI assistant specializing in automatic driving scene judgment. Your primary task is to analyze a given traffic scene and make a decision or evaluation based on it.

Input:

You will be provided with an image, a corresponding question, and a set of possible options.

Answering Guidelines:

- Your reasoning must be based on the visual evidence in the image and fundamental principles of safe driving.
- Analyze the situation step-by-step before making a final decision.

INSTRUCTION:

You should select one or more options from the given choices, outputting only the corresponding letters separated by commas.

Output Format:

Your response must be structured in a specific two-part format within a single turn. First, generate a structured Chain-of-Thought rationale enclosed within `<think>...</think>` tags; second, provide the final decision enclosed within `<answer>...</answer>` tags. The structure must be exactly:

```
<think>Your detailed reasoning process here.</think><answer>Your chosen option letter(s) here (comma-separated).</answer>
```

Prompt 2: Multiple-choice question — User Input Template

IMAGE: {image}

QUESTION: {question}

OPTIONS: {options}

Figure 13: System instruction and user input templates for the single-choice and multiple-choice Chain-of-Thought prompts.

Prompt 3: Error Tagging (Explainability) — System Instruction

You are an autonomous-driving evaluation assistant for multimodal (image + text) questions. Your job is to analyze a model's final answer and its detailed reasoning (chain-of-thought), detect which error patterns apply, and map them to the integer labels defined below. The user input will always contain: (1) the original question, (2) the question options, (3) the correct answer, (4) the model's final answer, (5) the model's detailed reasoning, and (6) an image associated with the question. Use both the image and the textual inputs (final answer + reasoning) to decide which label(s) apply.

Label definitions (0-9):

- 0 = Correct – The model's final answer is correct and its reasoning is sound and sufficient.
- 1 = Logical Reasoning Error – Perception may be correct, but the subsequent reasoning is logically invalid or contradicts traffic rules or causality.
- 2 = Semantic Feature Omission – The model overlooks or misjudges safety-critical semantic/visual cues (e.g., brake lights, turn signals, pedestrian gestures) or other discriminative attributes necessary for correct recognition and categorization.
- 3 = Model Hallucination – The model produces information inconsistent with the actual input (e.g., invents non-existent objects, attributes, or relations).
- 4 = Modality Imbalance – The model over-relies on one modality (text or image) while neglecting the other, causing an error.
- 5 = Spatial Relation Misjudgment – The model makes incorrect judgments about spatial relations (e.g., distance, relative position, depth).
- 6 = Limited Logical Inference – The model derives a decision from insufficient local evidence without integrating broader scene context.
- 7 = Generalization Deficit – The model generalizes poorly to rare or out-of-distribution scenarios (e.g., construction zones, traffic incidents, temporary lane closures).
- 8 = Decision Boundary Instability – Near critical operating points, small input perturbations cause large changes in the chosen action.
- 9 = Target Priority Misjudgment – The model fails to correctly prioritize among competing objectives (e.g., yielding to pedestrians vs. maintaining speed).

Classification rules:

- Use both the image and the provided text (final answer + reasoning) to decide labels.
- If the final answer is correct but the reasoning is flawed in any way, do NOT output 0; instead output the label(s) for the flawed aspects (you may include multiple labels).

Output format:

Your output must be ONLY a comma-separated list of integers (no words, no punctuation except commas and digits). Examples:

0
7
1,3
2,6,9

Prompt 3: Error Tagging (Explainability) — User Input Template

```
IMAGE: {image}
QUESTION: {question}
OPTIONS: {options}
ANSWER: {answer}
MODEL FINAL ANSWER: {model_answer}
MODEL REASONING: {reasoning}
```

Figure 14: System instruction and user input template for the explainability error-tagging prompt.

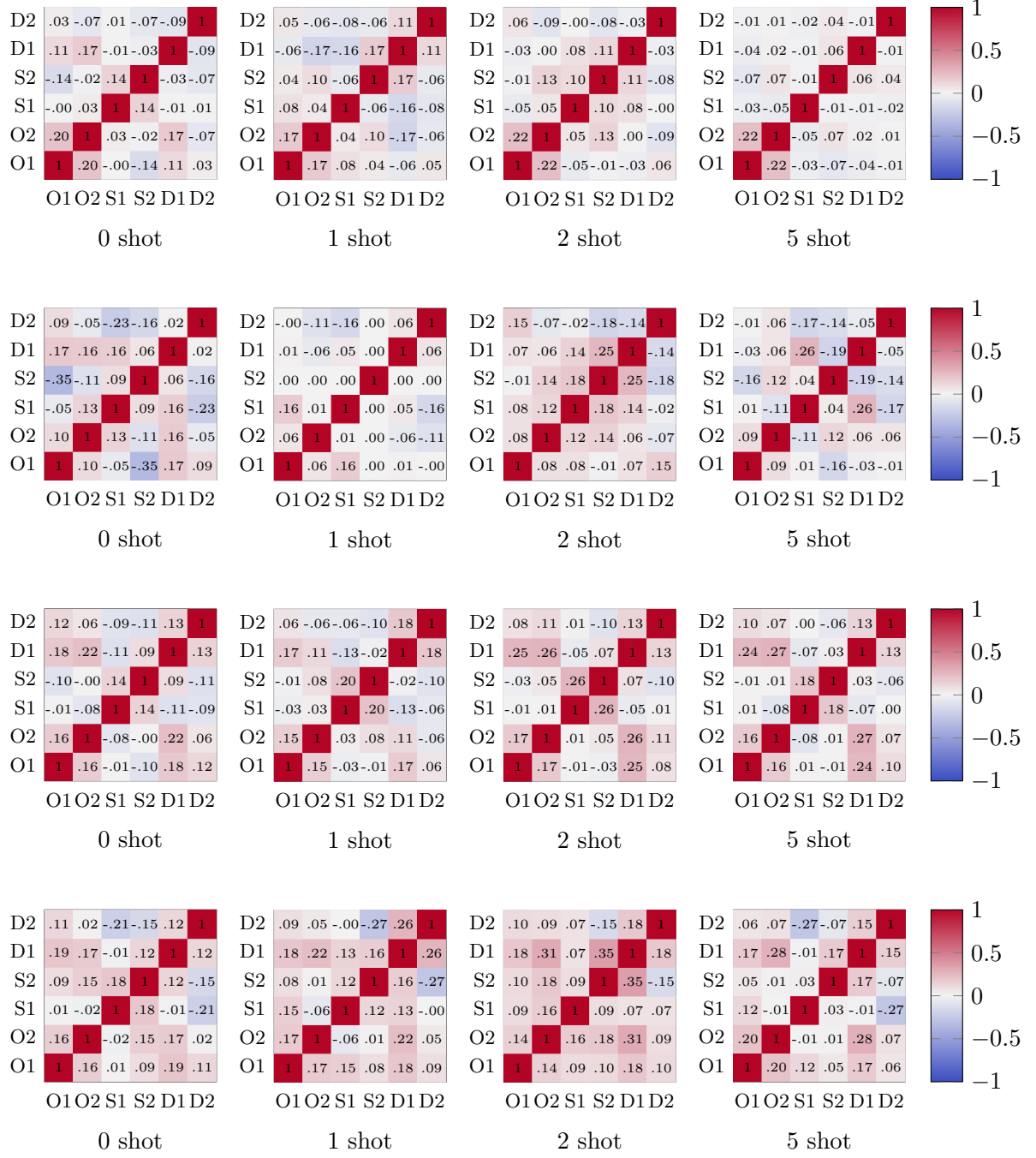


Figure 15: Correlation matrices across the six evaluation tasks—for Qwen (7B) and Qwen (72B). For each model, four panels correspond to prompt settings (0/1/2/5-shot). Rows and columns appear in the fixed order [O1, O2, S1, S2, D1, D2]; each cell reports the Pearson ϕ correlation between the binary correctness indicators of the two tasks, computed over the set of images common to both tasks (diagonal entries = 1). Colors encode correlation on a fixed range $[-1, 1]$ (blue \rightarrow negative, white ≈ 0 , red \rightarrow positive), with the numeric value overlaid in each cell.

Table 8: Evaluation on All Scenarios

Model	Size	Open	Shots	Object-1	Object-2	Scene-1	Scene-2	Decision-1	Decision-2	Avg Score
Gemini-2.5Pro	-	✗	0	62.90	74.35	76.73	25.61	49.47	55.11	57.36
			1	65.04	71.45	76.28	30.96	55.11	58.78	59.60
			2	62.14	71.76	81.18	39.12	51.30	45.80	58.55
			5	63.05	72.98	80.29	38.68	51.45	53.44	59.98
			0	67.48	73.74	92.54	46.44	56.95	51.91	64.84
GPT-4.1	-	✗	1	68.09	72.52	92.76	45.36	54.05	46.87	63.28
			2	69.16	73.89	93.21	45.36	54.81	46.87	63.88
			5	67.94	73.59	92.76	43.65	55.42	47.33	63.45
			0	49.86	50.07	27.34	0.89	45.78	30.66	34.10
Gemma	4B	✓	1	50.24	49.93	34.17	21.25	46.85	30.81	38.87
			2	50.99	52.26	7.28	17.14	45.64	37.68	35.17
			5	51.52	52.55	12.04	18.70	44.97	46.14	37.65
			0	64.46	63.55	63.45	7.20	50.40	31.65	46.78
Gemma	27B	✓	1	64.15	63.10	64.56	8.17	50.55	30.74	46.88
			2	64.22	63.62	64.94	10.11	50.02	30.43	47.22
			5	64.67	62.95	64.71	12.73	50.10	30.13	47.55
			0	58.67	53.45	87.00	18.37	41.84	37.99	49.55
Llama	11B	✓	1	45.86	46.65	22.29	0.07	34.12	39.18	31.36
			2	23.54	49.36	26.67	2.73	31.62	39.37	28.88
			5	40.59	42.78	20.95	2.92	26.94	37.40	28.60
			0	51.39	63.48	91.75	36.78	45.14	49.55	56.35
Llama	90B	✓	1	58.62	61.50	66.64	21.57	41.16	45.64	49.19
			2	56.61	65.58	83.06	30.79	37.48	43.05	52.76
			5	59.62	64.83	83.13	35.42	40.57	47.28	55.14
			0	26.23	52.95	87.15	32.49	41.40	29.87	45.01
Llava	7B	✓	1	26.59	47.59	72.51	7.31	34.34	42.17	38.42
			2	25.18	46.76	82.76	10.08	46.24	35.04	41.01
			5	25.69	50.19	85.88	16.19	49.90	29.20	42.84
			0	45.88	66.72	85.66	35.42	51.60	34.89	53.36
Llava	72B	✓	1	55.79	64.82	82.62	22.71	44.38	41.97	52.05
			2	47.17	66.04	86.41	35.86	45.84	34.21	52.59
			5	55.53	66.04	84.70	34.22	52.23	34.28	54.50
			0	60.23	63.10	91.01	21.67	44.58	30.72	51.89
Phi	6B	✓	1	62.71	53.80	82.09	13.35	39.37	39.07	48.40
			2	53.52	60.91	90.12	18.25	46.25	39.34	51.40
			5	62.02	59.70	85.51	24.15	34.34	46.09	51.97
			0	65.58	59.34	65.16	33.60	40.87	35.48	50.00
Qwen	7B	✓	1	59.03	61.69	41.38	14.07	45.28	36.02	42.91
			2	60.97	62.20	53.34	22.66	42.22	35.56	46.16
			5	60.37	62.36	54.16	30.04	43.81	32.45	47.20
			0	68.06	68.24	77.19	37.62	54.69	38.20	57.33
Qwen	72B	✓	1	68.53	68.76	77.05	45.07	54.17	42.31	59.31
			2	68.67	68.69	86.85	47.82	52.87	36.62	60.25
			5	68.67	68.38	87.59	48.98	53.47	38.13	60.87

Table 9: Evaluation on High-Risk Scenarios

Model	Size	Open	Shots	Object-1	Object-2	Scene-1	Scene-2	Decision-1	Decision-2	Avg Score
Gemini-2.5Pro	-	✗	0	77.40	70.62	75.00	23.68	63.84	77.40	64.66
			1	70.62	67.23	80.26	26.32	65.54	77.40	64.56
			2	73.45	64.41	81.58	36.18	55.93	60.45	62.00
			5	71.75	65.54	84.21	30.48	61.58	64.97	63.09
			0	80.23	68.93	92.76	48.90	71.75	68.36	71.82
GPT-4.1	-	✗	1	80.23	65.54	93.42	46.49	59.32	58.76	67.29
			2	83.05	66.10	93.42	45.18	62.15	58.19	68.02
			5	81.92	66.10	94.74	45.83	63.84	59.89	68.72
			0	67.62	37.05	24.14	0.00	55.88	36.34	36.84
Gemma	4B	✓	1	67.93	37.33	32.70	13.35	59.23	34.66	40.87
			2	67.90	41.52	7.21	11.68	59.57	50.28	39.69
			5	68.78	43.67	12.66	13.35	60.11	65.68	44.04
			0	67.74	56.11	64.37	2.64	58.78	38.43	48.01
Gemma	27B	✓	1	67.99	56.67	59.71	8.52	58.19	38.23	48.22
			2	68.89	56.73	62.26	10.28	58.19	35.36	48.62
			5	68.61	56.73	60.15	12.91	57.26	35.67	48.56
			0	63.37	42.08	86.82	16.13	37.70	51.04	49.52
Llama	11B	✓	1	52.50	40.49	23.09	0.00	65.34	54.30	39.29
			2	24.97	42.63	29.30	4.80	54.58	52.73	34.84
			5	44.00	36.49	28.47	5.33	51.15	54.98	36.74
			0	53.04	54.33	90.25	28.83	59.71	69.26	59.24
Llama	90B	✓	1	61.43	52.14	71.24	21.36	66.58	63.82	56.10
			2	58.45	58.81	88.93	25.14	60.70	58.98	58.50
			5	61.29	55.88	88.58	29.31	65.73	63.77	60.76
			0	9.37	48.37	86.02	19.78	21.37	27.37	35.38
Llava	7B	✓	1	10.64	36.32	83.13	2.34	65.34	61.82	43.26
			2	7.86	39.05	81.72	1.61	39.08	50.87	36.70
			5	7.91	43.78	85.99	11.01	50.25	27.99	37.82
			0	42.57	60.19	86.42	27.37	52.28	50.56	53.23
Llava	72B	✓	1	51.75	57.26	78.19	17.99	62.89	62.16	55.04
			2	43.41	59.32	87.70	29.04	63.25	50.11	55.47
			5	51.72	58.39	86.86	27.45	60.47	49.27	55.69
			0	55.89	51.88	91.13	19.87	26.36	35.48	46.77
Phi	6B	✓	1	61.63	42.46	86.11	12.10	64.19	53.07	53.26
			2	46.40	49.69	90.69	16.31	53.40	55.21	51.95
			5	55.18	47.72	85.11	23.16	64.78	65.14	56.85
			0	59.57	49.97	68.55	40.27	33.42	44.63	49.40
Qwen	7B	✓	1	50.87	51.83	34.68	11.12	58.33	45.02	41.98
			2	54.28	51.40	48.69	15.74	44.40	43.39	42.98
			5	51.41	55.21	48.37	22.83	45.84	39.53	43.86
			0	66.69	59.01	84.09	36.78	57.06	45.87	58.25
Qwen	72B	✓	1	67.80	58.19	76.16	45.91	60.19	51.74	60.00
			2	67.82	59.31	89.10	51.34	53.07	40.66	60.22
			5	67.09	58.28	89.19	47.21	55.21	40.46	59.57